



HAL
open science

Titan's neutral atmosphere seasonal variations up to the end of the Cassini mission

A. Coustenis, D.E. Jennings, R.K. Achterberg, P. Lavvas, G. Bampasidis,
C.A. Nixon, F.M. Flasar

► **To cite this version:**

A. Coustenis, D.E. Jennings, R.K. Achterberg, P. Lavvas, G. Bampasidis, et al.. Titan's neutral atmosphere seasonal variations up to the end of the Cassini mission. *Icarus*, 2020, 344 (1), pp.113413. 10.1016/j.icarus.2019.113413 . hal-02354914

HAL Id: hal-02354914

<https://hal.science/hal-02354914>

Submitted on 18 Nov 2020

HAL is a multi-disciplinary open access archive for the deposit and dissemination of scientific research documents, whether they are published or not. The documents may come from teaching and research institutions in France or abroad, or from public or private research centers.

L'archive ouverte pluridisciplinaire **HAL**, est destinée au dépôt et à la diffusion de documents scientifiques de niveau recherche, publiés ou non, émanant des établissements d'enseignement et de recherche français ou étrangers, des laboratoires publics ou privés.

Titan's neutral atmosphere seasonal variations up to the end of the Cassini mission

A. Coustenis¹, D. E. Jennings², R. K. Achterberg^{2,3}, P. Lavvas⁴, G. Bampasidis⁵, C. A. Nixon², F. M. Flasar²

¹Laboratoire d'Etudes Spatiales et d'Instrumentation en Astrophysique (LESIA), Observatoire de Paris, CNRS, Université Paris-Science-et-Lettres, Sorbonne Université, Université de Paris, 5, place Jules Janssen, 92195 Meudon Cedex, France

²Planetary Systems Laboratory, Goddard Space Flight Center, Greenbelt, MD 20771, USA

³Department of Astronomy, University of Maryland, College Park, MD 20742, USA

⁴GSMA, Reims Champagne-Ardenne, 51687 Reims, France

⁵School of Education, Department of Primary Education, National & Kapodistrian University of Athens, 10680 Athens, Greece.

Corresponding author: A. Coustenis, *Laboratoire d'Etudes Spatiales et d'Instrumentation en Astrophysique (LESIA), Observatoire de Paris, CNRS, PSL Univ., Sorbonne Univ., Paris Univ., 5, place Jules Janssen, 92195 Meudon Cedex, France* (athena.coustenis@obspm.fr)

Keywords: Titan; Titan, atmosphere; Satellites, atmospheres; Spectroscopy; Radiative transfer

*Second Revised version, submitted to Icarus Cassini Special Issue
6 August 2019*

Abstract

In this paper we report new results concerning the seasonal atmospheric evolution near Titan's poles and equator in terms of temperature and composition using nadir spectra acquired by the Cassini Composite Infrared Spectrometer (CIRS) at high spectral resolution during the last year of the Cassini mission in 2017 complementing previous investigations covering almost two Titan seasons. In recent previous papers (Coustenis et al., 2016, 2018), we have reported on monitoring of Titan's stratosphere near the poles after the mid-2009 northern spring equinox. In particular we have reported on the observed strong temperature decrease and compositional enhancement above Titan's southern polar latitudes since 2012 and until 2014 of several trace species, such as complex hydrocarbons and nitriles, which were previously observed only at high northern latitudes. This effect accompanied the transition of Titan's seasons from northern winter in 2002 to northern summer in 2017, while at that latter time, the southern hemisphere was entering winter. Our new data, acquired in 2017 and analyzed here, are important because they are the only ones recorded since 2014 close to the south pole in the mid-infrared nadir mode at high resolution. A large temperature increase in the southern polar stratosphere (by 10-50 K in the 0.1 mbar-0.01 mbar pressure range) is found associated with a change in the temperature profile's shape. The 2017 observations also show a related significant decrease in most of the southern abundances which must have started sometime between 2014 and 2017. For the north, the spectra indicate a continuation of the decrease of the abundances which we first reported to have started in 2015 and small temperature variations. We discuss comparisons with other results and with current photochemical and dynamical models which could be updated and improved by the new constraints set by the findings presented here.

1. Introduction

The Cassini-Huygens mission observed the Saturnian system for 13 years, covering about two Saturnian seasons and providing a wealth of data which yield considerable new information about the objects in the system. Among the kronian satellites, Titan offered the opportunity for many new discoveries in its system where the atmosphere, the surface and the interior are interconnected and evolve with the season (from early winter in the north at the beginning of the mission in mid-2004, until its end just after summer solstice in mid-2017). The last targeted Titan flyby was on April 23,

61 2017, in the beginning of Cassini Grand Finale orbits when the spacecraft started dipping between
62 the rings and the planet. The last non-targeted Titan flyby was on September 11, 2017 putting Cassini
63 on impact trajectory with Saturn. Among other, the atmospheres of the planet itself and Titan have
64 been investigated by the Cassini Composite Infrared Spectrometer (for the description of CIRS see
65 for instance Flasar et al., 2004 and Jennings et al., 2017). The data we present here pertain to the
66 stratosphere of Titan, above the poles and near the equator as observed from different trajectory points
67 in 2017 within the Grand Finale mission.

68 Several investigators have found variations in temperature and composition within Titan's
69 stratosphere both in a spatial and a temporal distribution. Seasonal variations from CIRS data obtained
70 during the duration of the Cassini mission were reported in numerous previous publications by this
71 team and other authors (e.g. Coustenis et al., 2007, 2010, 2013; Teanby et al., 2012, 2017; Vinatier
72 et al., 2015, 2018; Jennings et al., 2012a). This team has recently focused on analyses of spectra
73 acquired near polar latitudes by Cassini/CIRS at high resolution in the 600-1500 cm^{-1} range to infer
74 the composition and temperature of Titan's stratosphere probed at those wavenumbers (Coustenis et
75 al., 2016, 2018). In particular, fast and important seasonal effects have been observed in the
76 atmosphere of the satellite pointing to a large-scale reversal, which occurred in the single pole-to-
77 pole circulation of Titan's atmosphere after the northern equinox in mid-2009 and which led to gases
78 upwelling from the southern summer hemisphere and then downwelling at the northern winter pole
79 (Achterberg et al., 2008, 2011; Teanby et al., 2012; Bampasidis et al., 2012), significantly affecting
80 the temperature and the composition near the poles of Titan. It is noteworthy that all previous
81 investigations indicate that the polar and mid-latitude abundances show different trends indicating
82 different dynamical processes which occur inside and out of the polar vortex region, extending down
83 to about 50°S in latitude.

84 While most trace stratospheric gases in the north polar data generally show only a small
85 decreasing trend until 2014, the southern polar results on the contrary point to a strong enhancement
86 after 2012 (Coustenis et al., 2016, 2018). As argued also by other investigators (e.g. Vinatier et al.,
87 2015; Teanby et al., 2017), this indicates a fast and strong buildup of the gases in the southern pole
88 while it goes deeper into the shadow during the 2013-2014 southern autumn, as predicted by models
89 (e.g. Hourdin et al., 2004; Rannou et al., 2005; Lebonnois et al., 2009, 2012). This was associated
90 with temperature changes we have registered in our previous publications where from 2013 until
91 2016, the northern polar region has shown a temperature increase of 10 K, while the south has shown
92 a more significant decrease (up to 25 K) in a similar period of time. Jennings et al. (2012a, b, 2015)
93 found that the increase in gaseous content in the south is related to the haze increase that was also
94 seen in the south following its decrease in the north. As indicated in these previous publications, after
95 northern spring equinox in 2009, we discovered that the global dynamics in Titan's atmosphere
96 changed dramatically. Seasonal solar heating moved towards the north pole, where the vortex began
97 weakening, as indicated by the decrease in the equator-to-pole temperature gradient. At the same
98 time, in the south pole a hot spot was formed in the higher northern polar stratosphere leading to a
99 large enrichment of trace gaseous components, aerosols and condensates produced by photochemistry
100 (West et al., 2011, 2016; Jennings et al., 2012a,b, 2015; Coustenis et al., 2013; Teanby et al., 2017;
101 Vinatier et al., 2015, 2018). Thus, towards the end of that period, the strong gaseous signatures had
102 almost disappeared in the north, and similar features started to appear near the south polar stratosphere
103 which evolved with the season there heading towards winter.

104 The new 2017 stratosphere data we present here consist of eight selections in FP3 and FP4
105 above Titan's north pole at latitudes between 65°N and 90°N and six selections above the south pole
106 beyond 65°S. We have also analyzed a large spectral average around the equator. The selections are
107 described in Table 1. This paper then follows the Coustenis et al. (2016 and 2018) publications on
108 seasonal effects in the atmosphere, looking for the predicted and theorized changes in abundance of
109 the polar constituents. In Section 2 we describe our data and stress the importance of the selections
110 in 2017 that we analyze here, but we also include results from years after 2010. We also briefly
111 describe the method used in the analysis that has been applied to previous publications. Section 3 we
112 present our results and discuss the context within original and intriguing changes in the trends for the
113 atmospheric temperature and chemical structure are observed importantly complementing the
114 previous findings. In Section 4 we conclude and compare with existing photochemical and general
115 circulation models (GCM) pointing at constraints that could be useful in updating and improving
116 them.

117
118

119 2. Observations and data analysis

120
121
122

The data analyzed in this article were taken in 2017 by CIRS at high spectral resolution (0.5 cm^{-1}) in the surface-intercepting nadir mode. The Cassini CIRS instrument is described in Flasar et

Supprimé:

124 al. (2004) and Jennings et al. (2017). It consists of a Fourier transform spectrometer operating in the
125 10 to 1500 cm^{-1} spectral range, divided in three channels or Focal Planes (FP). Titan observations
126 with CIRS during the Cassini mission are described extensively in Nixon et al. (2019). Here, we use
127 the spectra acquired in the mid-infrared focal planes (FP3 and FP4) that cover the 600-1500 cm^{-1}
128 range. CIRS spectra in this spectral range probe the stratosphere which covers levels between roughly
129 100 and 400 km in altitude and pressure levels between 0.01 and 20 mbar essentially for the CIRS
130 nadir polar observations (Flasar et al., 2005).

131 In particular, since we require high-resolution nadir spectra of Titan's stratosphere near the
132 poles (from 65° to 90°), in order to separate the contributions of the different gas components (see
133 for example Coustenis et al., 2010), we have to point out that this type of dataset suffers occasionally
134 from lack of observations for high latitudes, caused by Cassini's orbital geometry (see Fig. 1 in
135 Coustenis et al., 2018 and also Nixon et al., 2019). Indeed, the north pole was not observed before
136 mid-2013 and between fall 2014 and May 2016. For the south pole we did not have enough high-
137 resolution (0.5 cm^{-1}) available spectra from fall of 2014 onwards and until 2017. The 2017 data that
138 we present here are then very important because they give us for the first time an indication to what
139 happened in the south polar stratosphere after 2014 and because they increase the number of
140 observations we can analyze in the northern pole region.

141 Figure 1 shows a comparison between the more recent (2017) CIRS spectra and the 2014 ones
142 in the 1100-1400 cm^{-1} range (FP4 focal plane, where the methane band is located) hinting to strong
143 changes having occurred since that time close to the South Pole. Indeed, a strong increase in the
144 emission in the CH_4 band in 2017 corresponds to a much hotter stratosphere in these later dates as
145 will be quantified below. See Fig. 2 of Coustenis et al. (2016) for indications of gradual enhancement
146 in Titan's south pole atmosphere from the FP3 spectra.

147 Table 1 shows the spectra used in this work for complementing our monitoring of the temporal
148 and seasonal evolution of Titan's polar thermal and chemical stratospheric structure, in particular
149 since 2012. In addition, we have included a large spectral average near the equator in order to compare
150 with previous inferences.

151 The field of view (FOV) of our CIRS observations was restricted to be entirely on Titan's disk
152 and emission angles were limited to 0 - 65° to avoid the need for large atmospheric corrections.
153 Available spectra within each time period were zonally averaged in large latitude bins covering
154 latitudes within the 65° to 90° latitude range. The averages depend on the data available for a given
155 date/flyby within a latitude range and aim at improving the signal-to-noise ratio (except for the
156 equatorial average which spans several dates from February to September 2017).

157 All of the 2017 spectral averages in Table 1 include spectra between 65°S and 90°S with
158 emission angles from 50 - 60 degrees and most of the spectra corresponding to 70°S . We have two
159 datasets near Titan's south pole in February 2017, one averaging data centered at 70°S and the other
160 southern average with spectra from 70°S - 90°S and emission angles from 30 - 60 degrees (with a much
161 larger (10 times) total number of spectra included), being more representative of higher latitudes
162 around 80°S .

163 As in previous papers, we use a monochromatic radiative transfer code adapted to Titan's
164 stratosphere (ARTT: Coustenis et al., 2010; Bampasidis et al., 2012). Updates are included in
165 Coustenis et al. (2010) and more recent publications and the method is extensively explained in detail
166 in Section 3 of Coustenis et al (2007). In brief, we use a line-by-line radiative transfer code to simulate
167 the observed Titan spectrum in FP3 and FP4 and through iterative processes we derive the
168 temperatures and the abundances of the various constituents observe in Titan's atmosphere. We infer
169 the temperature profile from the best fit of the 7.7-micron methane band in FP4 (following the method
170 described in e.g. Achterberg et al., 2008) which performs inversions of the emission observed in the
171 ν_4 methane band assuming 1.48% of CH_4 in the stratosphere increasing below the cold trap to about
172 5% at the surface as measured by the Huygens Gas Chromatograph Mass Spectrometer (GCMS) and
173 compatible with the CIRS inferences from FP1 (Flasar et al., 2005; Niemann et al., 2010). The
174 spectral modelling method for the temperature retrievals is described in Achterberg et al. (2008).
175 Temperatures are retrieved using the constrained linear inversion algorithm of Conrath et al. (1998)
176 using the spectral range from 1251 to 1311 cm^{-1} within the ν_4 band of methane. The methane
177 absorption is calculated using the correlated-k approximation (Lacis and Oinas, 1991) with methane
178 absorption data from HITRAN 2012.

179 Figure 2 shows the fitting of the methane ν_4 band in the 1250 to 1350 cm^{-1} region. In our
180 model the temperature profile is originally set to the one measured by CIRS emission values in the
181 7.7 micron CH_4 band and from lower resolution observations and then inverted to fit the FP4 spectrum
182 (Achterberg et al., 2008, 2011; Coustenis et al., 2007, 2010, 2016; Bampasidis et al., 2012).

183 We then inject the temperature profile in our ARTT radiative transfer code and solve for the
184 opacity in the rest of the spectrum retrieving the abundances of trace gases and their isotopes in the
185 FP3 region of the CIRS spectra (for a full list of molecules included in our simulations and the

Supprimé: sperate

187 associated spectroscopic parameters see previous publications and Table 2 in Jennings et al., 2017).
188 Figure 3 shows two of our fits in the 600-1000 cm^{-1} range, where we observe the emission of several
189 gaseous bands of hydrocarbons, nitriles and oxygen compounds (e.g. HCN, C_2H_2 , C_3H_8 , C_2H_6 , CO_2).
190 We apply constant-with-height vertical profiles from the higher levels of the atmosphere (around 400
191 km in altitude) down to the condensation level and then follow the saturation curve. Our spectra were
192 taken in the nadir mode and we lack information on the altitude dependence of the mixing ratios. This
193 assumption is essentially valid for all the molecules considered here, due to their weak emission
194 bands, except for C_2H_2 whose abundance variations with height are taken into account by making use
195 of weighted averages over the P, Q and R branches of the 729 cm^{-1} band and by testing vertical
196 profiles as described in detail in Bampasidis et al. (2012). We then infer mixing ratios that are
197 constant-with-height above the condensation level and correspond to the atmospheric pressure levels
198 indicated by the contribution functions in Figure 4.

199 The uncertainty on our inferences is determined as explained in previous publications and in
200 particular in Coustenis et al. (2010) and Bampasidis et al. (2012) with details. The uncertainties due
201 to the measurements noise is small because the NESR (Noise Equivalent Spectral Radiance) is
202 generally on the order of some 10^{-9} as shown in Figure 23 of Jennings et al. (2017) for our spectral
203 range, which combined to the large number of spectra summed, gives noise levels of some 2 to 4
204 orders of magnitude smaller than the radiance in our averaged spectra. Thus, we take into account, as
205 before, uncertainties due only to continuum fitting, temperature inferences and calibration.

206
207

208 3. Results and discussion

209

210 In our recent publication (Coustenis et al., 2018), we inferred the temperature profiles and the
211 chemical composition at different dates from 2012 and up to 2016 for high northern and southern
212 latitudes (at and beyond 65°N and 65°S). We here add the new calibrated and processed data from
213 2017.

214 In our previous papers, as well as in those of other investigators, it has been discussed how
215 as the southern hemisphere moved into autumn after the mid-2009 equinox, large temperature
216 variations were observed near the south pole (beyond 60°S) in the stratosphere (essentially from 0.1
217 down to 1 mbar). Indeed, while a moderate warming was observed in the summer-entering north for
218 the mid and high northern latitudes, a spectacular drop in temperature by as much as 25 K at 70°S
219 was measured from 2012 to 2014 in the stratosphere of Titan at levels around 0.3 mbar (Coustenis et
220 al., 2016). Since 2014, we had no high-resolution nadir data in FP3 and FP4 to exploit for temperature
221 and composition of the south pole, which now is feasible with the 2017 measurements. The previous
222 temperature variations were accompanied by a strong enhancement of chemical compounds in the
223 south polar region, while the north failed to show the opposite effect in a similar magnitude, which
224 indicated a non-symmetrical reaction to the seasonal influence for each pole. In our 2018 paper, we
225 showed how the north polar stratosphere only responded with a decrease of the chemical content after
226 2015, a three-year delay with respect to the increasing south. We explore here more recent dates
227 seeking to determine longer-term seasonal effects near Titan's poles by the use of the 2017
228 observations.

229

230 3.1 Thermal Structure Variations in the Stratosphere Near the Poles from 2012 to 2017

231

232 In order to determine which atmospheric levels our results pertain to, we have calculated and
233 show in Figure 4 the contribution functions for the methane (and hence for the temperature retrievals)
234 and for the other molecules investigated in this paper from 2010 to 2017. Our contribution functions
235 up to that time indicate that the emission observed in the 7.7-micron methane band (observed in CIRS
236 FP4 from 1250 to 1350 cm^{-1} roughly when the P and R branches are taken into account and centered
237 at 1304 cm^{-1}) originate essentially and in general from levels 0.01-20 mbar (70-400 km in altitude:
238 Fig. 5a,b).

239 Our contribution functions for the southern latitudes (Fig. 4, two left columns) from the
240 methane emission in the Q-branch and its wings indicate that at 70°S the emission in the methane
241 band sounds pressure layers around 0.4 mbar (180 km) for the earlier dates and higher levels 0.2 to
242 0.02 mbar, peaking at around 0.05 mbar (300 km) in 2017. Indeed, the south polar temperature
243 structure (Fig. 5a) shifts the contribution function upwards so that much of the temperature sensitivity
244 is at about 0.05 mbar, but the line wings are still sensitive to the temperatures down to the 10-mbar
245 level (Fig. 4).

246 On the other hand, for the northern pole, the profiles we infer correspond to pressure levels
247 between 0.01 to 10 mbar, with weak variations with time, as supported by the small changes found
248 in the north pole temperature structure in the recent years (Fig.5b). The peak of the contribution

249 functions in the north indicates sounded levels around 0.1 mbar (0.05-1 mbar: 150-300 km), close to
250 the part of the atmosphere corresponding to the more recent southern profiles.

251 For the other gaseous species, the emission of the trace gases close to the south pole originates
252 from around 10 mbar but also from higher atmospheric levels around 0.5 mbar. The northern
253 observations on the other hand probe similar altitudes /pressure levels in the recent years, somewhat
254 higher than for the southern latitudes, depending on the molecule as shown in Fig. 4.

255 In Figure 5 we then show the stratospheric temperature on Titan beyond 65°S for different
256 years in different colors from 2010 to 2017 and similarly poleward of 65°N and different colors for
257 different dates from 2013 to 2017, comparing the temperature profiles inferred in this study from
258 2017 data with previous inferences (Coustenis et al., 2018) to derive a description of the thermal
259 evolution in the last 7 years of the Cassini mission.

260

261 *Temperature evolution near the southern pole*

262

263 Starting with the southern latitudes, we have previously reported on the dramatic temperature
264 decrease from 2010 to 2014 by more than 40 K at the 0.5 mbar (starting from around 170 K) and the
265 related consequences on the gaseous abundances (Coustenis et al., 2016, 2018). We recall that after
266 mid-2014 and until 2017 no nadir high-resolution CIRS data for the south pole were available in FP3
267 and FP4, highlighting the importance of the new 2017 data that we examine here. As can be seen in
268 Fig. 5a, the temperature profiles that we have retrieved from the 2017 February and June 70°S
269 observations, probing essentially levels around 0.05 mbar (0.02 and 0.2 mbar), are very different in
270 shape from the previous inferences, which showed a rather homogeneous to a small positive slope
271 with pressure in the stratospheric temperature distribution until 2014. The new profiles significantly
272 accentuate the trend with a much steeper positive slope in the stratosphere above about 150 km ($p < 1$
273 mbar) and up to 300 km (0.05 mbar). The lower-altitude parts of the high south temperatures for
274 February 2017 (Fig. 5a, black line) are located between the 2013 and 2014 ones we have previously
275 derived up to 0.5 mbar and even the June 2017 profile (Fig. 5b, red line) rests within the values
276 reported after 2012 up to about 0.2 mbar. However, it must be noted that, taking into account the
277 steeper-slopes of the 2017 profiles and the higher altitude levels probed in the southern data, we find
278 higher temperatures at 70°S than previously reported and on average, the south pole appears to be
279 returning to the warmer values found in 2010 and perhaps even more. Between February and June
280 2017, the Titan stratosphere gains about 15 K in the 0.5 mbar to 0.1 mbar region. Titan's southern
281 polar stratosphere 2017 data indicate that the temperature is fast increasing above 0.5 mbar, and has
282 gained at least 35 K with respect to 2014 up to 0.1 mbar, while in June 2017, the increase is even
283 more impressive with temperatures attaining 150 K around 0.5 mbar and even joining or exceeding
284 the thermal values of the northern polar region above 0.1 mbar, arriving at 190 K. Such temperatures
285 in the higher stratosphere are now warmer than even in 2010 by 15 K or more. After a gap of about
286 2.5 years, the thermal increase in the south represents about +5 K in February 2017 to +30 K in June
287 2017 with respect to the September 2014 values.

288 Therefore, the stratosphere over the south pole of Titan shows dramatic increase in
289 temperature in 2017 since 2014, by 10-50 K in the 0.5 mbar-0.05 mbar pressure range, the larger
290 2017 temperatures observed in the higher atmospheric levels around 0.05 mbar. Achterberg et al.
291 (2019, in preparation) also report a noticeable warming of the south polar upper stratosphere ($p < \sim$
292 0.5 mbar) sometime between 2014 and 2016 using the temperature cross-sections from all the post-
293 equinox Titan flybys with mid-infrared maps that step across multiple latitudes with N/S to Saturn
294 oriented focal planes (MIRTMAP) covering both poles.

295 As shown in Figure 5a, the February 2017 data near the south pole could afford us two
296 different selections (this is the only occasion where we could recover enough spectra to make
297 averages with sufficient signal-to-noise, from 65 to 70°S or from 70°S to 90°S) and we derived two
298 different profiles centered at 70°S and 80°S (Table 1 and grey and black lines in Fig. 5a) which show
299 the 80°S being about 10K colder than the 70°S at around 0.5 mbar. The difference between the two
300 retrieved profiles is due mostly to latitudinal temperature gradients, the higher southern latitudes (i.e.
301 closer to the South Pole) remaining colder than the lower ones. If this is true, the difference between
302 the temperature profiles for the large averages of February and June 2017, could also possibly be due
303 at least partly to looking at slightly different latitudes, rather than reflecting temporal changes over 4
304 months.

305

306 *Temperature evolution near the northern pole*

307

308 Turning to the northern pole and comparing our new data with the earlier dates at 70°N in Fig.
309 5b, we still find relatively moderate changes. We had previously reported a 10 K increase from 2013
310 to 2016 (Coustenis et al., 2018), the north polar region's temperature starting to show an increase in

311 reaction to the augmented sunlight as the north moves towards summer with a three-year delay with
312 respect to the southern pole. Our 2017 temperature profile is very similar to the 2016 one in shape
313 and values and confirm that Titan's stratosphere has become warmer by up to 10 K in the 0.05-1 mbar
314 range, but given the uncertainties the changes could be much smaller. At lower pressure levels
315 (altitudes higher than 250 km), the 2017 profiles seem to be a little colder than during the 2013-2014
316 period, but all in all and within error bars the 2016 and 2017 profiles are very similar and up to 10 K
317 warmer than the earlier years (2013-2014) at around 1 mbar.

319 *Titan's thermal structure at the poles*

320
321 The two Titan poles then do not appear symmetrical in thermal response in the stratosphere
322 (Coustenis et al., 2018, and Fig. 5 here) in view of the dramatic decrease in the stratospheric
323 temperature in the south being initiated as early as 2012 (Coustenis et al., 2016). Our temperature
324 profiles are quite compatible with the results of limb observations at various dates published by
325 Teanby et al. (2017) for high southern latitudes and who also report on the post-equinox (after 2010)
326 hot spot found in Titan's upper stratosphere and the ensuing large compositional enrichment over the
327 following years and the associated thermal cooling as we have done in previous publications. These
328 authors find that the middle stratosphere and lower-stratosphere of Titan (around 200 km) above 80°S
329 has gradually cooled from 170 K in 2010 to 130 K in 2015. This is remarkably consistent within
330 uncertainties (both due to measurements and to spatial differences) with our results from Coustenis
331 et al. (2016, 2018) as shown in Fig. 5 where also our temperatures for high southern latitudes in 2010
332 start from around 170 K at those altitudes and finishes at around 125 K in September 2014 (our last
333 observation date before 2017). Teanby et al. (2017) also describe temperature changes at higher
334 altitudes, around 400 km, with an initial warming up to 180 K in late 2011 at 80°S (we find
335 temperatures around 170 K in late 2010), which drops by about 25K by early 2015 (we reported a
336 cooling down to about 155 K in September 2014). Teanby and colleagues report a heating up again
337 at these higher levels by late 2015, while the lower stratosphere remains stable and colder at around
338 125-130 K. This is in agreement with our findings.

340 *Temperature evolution near the equator*

341
342 We finally looked at the thermal structure near the equator from a large average of 2017 data
343 in the -10 to +10 latitudes (Table 1). Consistently with previous findings, the temperature profile for
344 the equator is more homogeneous with altitude and similar in shape to the earlier southern profiles
345 (e.g. June 2012), albeit considerably hotter at $p \gg 0.5$ mbar, increasing with altitude and situated
346 around 170°K at $p \ll 0.5$ mbar. Comparing this temperature profile in the 0.01-10 mbar range with
347 the one derived from 2004-2005 averages at 5°S and shown Fig. 4 of Coustenis et al. (2007), we find
348 a very clear stability of the equatorial thermal structure over the mission duration with temperatures
349 around an average of 170K in that pressure range.

352 **3.2 Variations of the Chemical Composition in the Stratosphere near the poles from 2012 to**

353 **2017**

354
355 It has been previously shown that as seasons shift on Titan, the strong changes witnessed in
356 temperature near Titan's poles, are usually accompanied by a decrease or an increase in radiative
357 emitters. The latter has already been observed and reported previously for somewhat lower latitudes,
358 for instance around 50°N, a latitude located at the border of the northern vortex. As indicated in
359 previous publications from CIRS data (e.g. Teanby et al., 2012; Vinatier et al., 2015; Coustenis et al.,
360 2018), temperature and composition changes took place essentially in the south pole in these past
361 years, with a strong enhancement observed for several of the species in the atmosphere as the southern
362 pole entered into autumn after 2010. Indeed, a couple of years after Titan's northern spring equinox
363 in mid-2009, the stratospheric dynamics on Titan featured a global reversal as the south pole was
364 entering fall, leading to a substantial enrichment of the trace gases within the southern pole vortex
365 created by subsidence from 2012 onwards. According to current General Circulation Model
366 models, this single circulation cell pattern should persist until 2025.

367 While the northern winter vortex was shown to be weakening and finally disappeared in the
368 past years (Coustenis et al., 2013; Jennings et al., 2015; Teanby et al., 2017), the nadir temperature
369 data from the 3 cm⁻¹ temperature maps shows that the southern vortex became broader sometime
370 between late 2014 and late 2016: the peak wind velocity and temperature gradient shifted from 70S
371 to ~45S, but the maximum wind velocity remained about the same or slightly lower (Achterberg et
372 al., 2019). The results by Teanby et al. (2017) from 2015 and 2016 measurements suggest a small

Supprimé: na

374 decrease of gases at the highest altitudes due to this broadening of the south polar vortex and to the
375 dilution of the enriched gas. The trace gas retrievals here then agree in indicating a weakening of the
376 subsidence in later dates.

377 Indeed, as we had no exploitable high-resolution nadir FP3 and FP4 data between late 2014 and
378 2017, we find here that the strong increase in temperature over the south pole in 2017 with respect to
379 2014 is associated with a significant and rapid drop in chemical content near the south pole (Figure
380 6). We thus witness in Titan's south pole the negative evolution or even disappearance of several
381 trace species, such as HC₃N and C₆H₆, previously observed clearly at high southern latitudes (for a
382 precise description of the lifetimes of the gaseous species in Titan's stratosphere see Section 4 of
383 Coustenis et al., 2016). This is due to the seasonal change on Titan, moving from northern winter in
384 2004 to advanced northern spring in 2012 and towards summer solstice in mid-2017, with the
385 opposite effect in the south pole as it moves into winter. The effect of this seasonal evolution is
386 predicted to be a reversal of the circulation cell allowing for gaseous components to move from the
387 equator to the South (see e.g. Teanby et al., 2012).

388 Fig. 6 shows our findings for the abundances of the minor gaseous components near both poles,
389 with a maximum of the contribution functions in the 0.1-10 mbar range (90-250 km). We have omitted
390 CO₂, which shows no significant variations in 2017. The blue lines in Fig. 6 represent the south polar
391 latitudes around 70°S and show increase in the abundances by one or several orders of magnitude for
392 many gases until the end of 2014, as described in Coustenis et al. (2018).

393 First, we compare our 2017 equatorial gaseous abundances (green points in Figure 6), with
394 those we have measured during the Cassini mission starting almost two seasons earlier (e.g. Coustenis
395 et al., 2007; 2010; Bampasidis et al., 2012; Vinatier et al., 2015, 2018). In 2017, the data provide only
396 an upper limit in C₆H₆ abundance of about 1×10^{-10} , which is comparable to values of about $1-2 \times 10^{-10}$
397 found throughout the mission, when the benzene signature was detectable. Similarly, for HC₃N, its
398 abundance is about 10^{-10} in 2017 and varies from 1 to 3 times that value throughout the mission, when
399 appearing. CO₂ has been quite constant at equatorial latitudes in the past 13 years and the value found
400 in 2017 ($1.5 \cdot 10^{-8} \pm 0.5 \cdot 10^{-8}$) is very close to the one reported in 2004, as it is also quite compatible
401 with the values reported at higher latitudes. The same applies for C₂H₂, C₂H₄, C₂H₆, C₃H₄ and C₄H₂,
402 which have remained close to values of about 3×10^{-6} , 10^{-7} , 8×10^{-6} and 5×10^{-9} , and 1.2×10^{-9} . Only
403 HCN and C₃H₈ show a deviation from their 2004 values here. Propane seems to have increased in the
404 past 13 years with more recent equatorial values consistently being 2-3 times higher than at the
405 beginning of the mission. HCN on the other hand has shown some decrease in the latter season by
406 about a factor of 2. We note that HCN and C₃H₈ are long-lived photochemical species, more potent
407 to changes inflicted by solar cycle modulations of the incoming insolation over the 13 years of Cassini
408 observations. Thus we believe these differences in the equatorial abundances of these species are a
409 subtle demonstration of this effect. Photochemical models assuming solar maximum and minimum
410 insolation demonstrate that the anticipated changes in the abundances of HCN and C₃H₈ are factors
411 of ~2 with higher insolation resulting to increased abundances for HCN and reduced for C₃H₈ (Lavvas
412 2007; Vuitton et al., 2019). The solar insolation was higher in 2004 compared to 2017
413 (<http://lasp.colorado.edu/lisird>), however the flux difference between the two years discussed here
414 (2004, 2017) is smaller than the maximum differences occurring from solar minimum (2009-2010)
415 to solar maximum (2014-2015). Therefore, the models appear to be qualitatively consistent with the
416 observations, yet further evaluations of the temporal evolution of the abundances may reveal further
417 details of the impact of the solar cycle. The Cassini observations presented here provide significant
418 constraints for the validation of such simulations. However, on the whole, the equatorial latitudes
419 seem to be much less affected, if at all for most molecules, by the changes in seasons.

420 As Figure 6 (red lines) shows, we find that all trace gases in the Titan north polar area have
421 decreased from September 2013 to August 2017, except for CO₂ which remains constant within error
422 bars and is not shown on this plot. Propane (C₃H₈) has shown a trend for decrease until 2016, but
423 from more recent data and within error bars we see no additional decrease of its abundance in 2017,
424 where it remains at around 1.5×10^{-6} .

425 In this 4-year period, we find the decrease we had announced in Coustenis et al. (2018) near the
426 northern polar region to be confirmed and prolonged. In total, from the abundances around the
427 beginning of 2014, when the north polar stratosphere was stable with enhanced species, until
428 September 2017 (about 3 years time), we witness a drop in content of various trace gases as follows:

- 429 • C₂H₂, C₂H₆ and C₃H₄ decrease by factors of about 2-3.
- 430 • For C₂H₄ and C₄H₂ the abundances decrease by factors of about 3.5-5.
- 431 • We find HCN and HC₃N to be less abundant by more than an order of magnitude
- 432 • C₆H₆ decreased until the end of 2016, but it seems to have stabilized during the first half
433 of 2017 at around 0.1 ppb, which is 5-7 times lower than in early 2014. Then it seems to
434 be slightly increasing again since mid-2017, reaching similar values as 4 years ago, by the
435 end of 2017. Although this increase appears real in view of the error bars, one should be

Supprimé: red

Supprimé: 4

438 cautious because of the difficulty in extracting the gaseous benzene contribution from the
439 area around 674 cm^{-1} , due to the interference from other species like C_2H_2 and HCN , which
440 have bands with strong spectroscopic signatures.

441 The north polar region has thus continued to become rarified in most of the stratospheric gases
442 (exceptions are CO_2 and C_3H_8), with the hydrocarbons somewhat less affected than the nitriles HCN
443 and HC_3N , who are reduced by more than an order of magnitude.

444 CO_2 and C_3H_8 find their abundances undiminished with respect to previous years in the North
445 as for the other molecules. CO_2 is a chemical product with extremely large photochemical life time,
446 while we do not have a clear picture of its behavior from the GCM results discussed in section 4.
447 C_3H_8 is one of the most abundant molecules where the abundance retrieval is complicated due to the
448 emission signature being mixed with the C_2H_2 one, which has more emission.

449 In the south pole, where we had no data since 2014, and following the rapid huge enhancement
450 of the chemical species from 2012 to 2014 (e.g. as described in Coustenis et al., 2016, 2018; Vinatier
451 et al., 2015; Teanby et al., 2017), we now report a strong decrease. All the molecules (except for CO_2)
452 have dropped with respect to the end-of-2014 peak at latitudes near 70°S and are now at abundance
453 levels close to the ones witnessed in 2013 (Figure 6, blue lines). This corresponds to the results we
454 have in the thermal profile which, as indicated in section 2, has returned for these southern latitudes
455 to values close to those found at dates around 2012. We do not know if the southern latitudes
456 abundances increased further after 2014, and when exactly the decrease began, but sometime after
457 2014, a significant decrease started in the south. Our two data points in 2017 (February and June at
458 70°S) confirm this is the case for all molecules with significant drops in mixing ratio, with the
459 exception of C_3H_8 and CO_2 , which show no real differences since 2014.

460 The new 2017 values indicate that since the peak found in September 2014 Titan's stratosphere
461 above around 70°S suffered a considerable loss in abundance as follows:

- 462 • C_2H_2 , C_2H_6 , C_3H_4 and C_4H_2 were reduced by factors of 1.5-2.
- 463 • C_2H_4 and C_6H_6 , although difficult to infer, show nevertheless very strong decrease in
464 abundance in 2017 with a drop by one and up to two orders of magnitude respectively. The
465 latter (C_6H_6) is currently almost showing the same value at some 10^{-9} near both poles.
- 466 • HC_3N has also lost 1.5 orders of magnitude in abundance, dropping close to its northern
467 value of about 10^{-9} . HCN is the most dramatically affected near 70°S with its mixing ratio
468 reduced by 2.5 orders of magnitude, down to some 6×10^{-7} , while it had reached values of
469 about 2×10^{-4} towards the end of 2014.

470 As said above, we had the opportunity in February 2017 to recover another average of spectra
471 at even higher latitudes centered around 80°S (as described in Table 1). The analysis of this dataset
472 is shown with black points in Figure 6. In all cases the spectral averages closer to the southern pole
473 on that specific date show higher values than the ones at 70°S . Since there is a fairly strong
474 temperature gradient with hotter temperatures between 60° and 90°S in the upper stratosphere, the
475 differences in abundances could be due to these discrepancies tied with the temperature changes
476 described in Section 3.1. This again points to the possibility that the southern stratosphere closer to
477 the pole maintains some of the larger abundances and it has not lost as much of its content as the
478 lower latitudes. The decrease in chemical species might then be affecting first lower latitudes before
479 reaching the pole.

480 We have to note again that we do not know if these decreases are the largest that affected Titan's
481 stratosphere above around 70°S , as we did not have any high-resolution FP3 nadir data between the
482 end of 2014 and the beginning of 2017 roughly. But they bring the indication that Titan's southern
483 polar region became subject to strong seasonal variations between autumn equinox and winter
484 solstice, while in 2014 Titan was in the middle of autumn in the south. We have already compared
485 our findings (as much as possible given the differences in mixing ratio inferences : constant-with-
486 height vs vertical distributions) to the results from the analysis of high southern limb spectra up to
487 dates in 2016 by Teanby et al. (2017), and indicated that for the dates we had previously exploited in
488 our 2016 and 2018 papers, the abundances are very compatible for all molecules except for the nitriles
489 where we find higher values (Coustenis et al., 2018, Section 3.2).

490 Other investigations, in particular using the Focal Plane 1 (FP1: $10\text{-}500\text{ cm}^{-1}$) spectral part of
491 the CIRS Titan data have also shown that the meridional distribution evolution of temperature and
492 chemical composition from northern winter (2004) to summer solstice (2017) denote important
493 seasonal changes in the lower stratosphere (between 10 and 20 mbar). This is especially true, as
494 reported from these mid-infrared analyses at the South pole (close to 70°S), where temperature
495 decreased by 24 K at 6 mbar and by 19 K at 15 mbar within 4 years from 2012 onwards (Sylvestre et
496 al., 2018, 2019).

497 Teanby et al. (2018) present an analysis of data acquired with ALMA in March 2017, and
498 among other they present profiles for C_3H_4 extracted from a Titan disk-average spectrum. Since in
499 2017 we find the northern and the southern constant-with-height mixing ratios of C_3H_4 (Fig. 6) to be

500 quite similar with values around 10^{-8} , we deduce a compatibility with the results of Teanby et al., who
501 have a similar average value in their two-point profile from 100 to 300 km in altitude around and a
502 somewhat lower abundance in their uniform profile. These results confirm the moderate decrease in
503 abundance for methylacetylene since the end of 2014 in the south compared to the decrease in other
504 molecules, also noted by Teanby et al (2018) who point at the similarities with the values from
505 Vinatier et al (2015). Our error bars in Fig. 6 indeed show that the 2017 C_3H_4 abundances can be
506 compatible with the values in the period 2014-2015.
507
508

509 **4. Conclusions and interpretations**

510 We discuss here the global picture of seasonal temperature and chemical composition variations
511 in the stratosphere near Titan's poles from 2010 to 2017, while Titan moved from northern winter in
512 2004 to advanced northern spring in 2012 and towards summer solstice in mid-2017, with the
513 opposite effect in the south pole as it moves towards winter. During that time, Titan's main
514 atmospheric circulation cell is expected to reverse and models predict that newly produced
515 photochemical species are channeled from mid latitudes towards the south pole (e.g. Teanby et al.,
516 2012). Where we have data, we searched for signatures of trace stratospheric gases in large spectral
517 averages around the poles and determined their abundances.
518

519 Our previous results had shown that the southern pole of Titan became substantially enhanced
520 in trace gases after 2012 and has dramatically decreased in temperature in 2012-2014 (Figure 5). The
521 situation has reversed in 2017 with the temperatures increasing and the chemical content decreasing,
522 as also witnessed in medium-resolution data (Achterberg et al., 2019, in preparation). In the North,
523 we had found that the composition decrease expected to compensate for the strong enhancement in
524 the South only set in about 3 years after the south had begun to become enriched (roughly 2015 vs
525 2012) and continues in 2017.

526 The general characteristics of our temperature and composition retrievals in this period (as
527 found also by other investigators, e.g. Vinatier et al., 2015) are in agreement with the broad features
528 of Titan's atmospheric circulation derived by GCM models (Lebonnois et al., 2009). These results
529 demonstrate that between vernal equinox and summer solstice the circulation pattern changes from a
530 two-shell circulation with upwelling at the equator and descending at the poles, to one global shell
531 circulation ascending from the summer pole and descending to the winter pole. The transition period
532 between these two patterns is 3 terrestrial years which means that by the end of 2012 a global pole to
533 pole circulation is established. This is the time when the increase in the south pole abundances is
534 observed. However, the latest south pole observations from 2017 reveal a different trend in both
535 temperature and composition from that established up to 2014. As shown in Fig. 6, in the past years
536 we see in the southern polar region the gradual but rapid decrease to almost disappearance of several
537 trace species among the complex hydrocarbons and nitriles, previously notoriously found there. This
538 is associated to a remarkable increase in temperature at the south pole in 2017 as compared to 2014
539 (Fig. 5a). As the species with the strongest drop in abundance are important infrared emitters, the
540 correlation with the increase in temperature is consistent with theoretical anticipations (Teanby et al.,
541 2017). On the contrary, the north pole becomes increasingly rarefied while its temperatures present
542 smaller variations warming by about 5-10 K near 1 mbar.

543 We can compare the general picture of Titan's seasonal changes observed with CIRS to the
544 corresponding evolution of polar temperature and composition from the Titan GCM database that
545 describes a coupled picture of circulation, photochemistry and haze microphysics (Rannou et al.,
546 2005). We note that the GCM results discussed hereafter were derived based on pre-Cassini data, thus
547 have not benefited to any degree from the plethora of new observational constraints as well as the
548 improvements that the new constraints have induced on our understanding of the physical and
549 chemical processes in Titan's atmosphere over the last 15 years. As noted in most recent publications
550 concerning GCM models for Titan's atmosphere (e.g. Lebonnois et al., 2012, Lora et al., 2015), there
551 is no complete study of the predictions on the seasonal variations of the Titan chemical composition
552 in the stratosphere. Thus, our goal with this comparison is to demonstrate the aspects that need to be
553 improved in the future applications of GCM models, based on the Cassini CIRS observations.

554 In Figure 7 we present the seasonal evolution of the mixing ratios over the polar regions
555 normalized to the 2010 and 2013 observations for the South and North pole, respectively. We resolve
556 to this relative comparison and not to a direct comparison of mixing ratios in order to focus on the
557 impact of the dynamics on the chemical composition. According to the GCM simulations the polar
558 abundances depend on the interplay between the influx of photochemical products in the winter polar
559 region by the Hadley cell, and the loss of these species in the lower stratosphere due to condensation,
560 while chemical effects have a secondary role in the resulting temporal evolution of the chemical
561 abundances (Hourdin et al., 2004). As seasons change the advection of material to the poles, as well

562 as, the thermal structure (therefore the condensation rates) change, resulting to different polar
563 enhancements. The atmospheric location probed for each species (contribution function) further
564 affects the degree of temporal variation observed over the seasons. Therefore, we used the
565 contribution function derived in our studies over different times (see Fig. 4) as a reference time-grid
566 on which we interpolate to derive the contribution function for each species at the reference times of
567 the GCM database (resolution of ~1 Earth year). With these contribution functions we calculate the
568 average mixing ratio of each species for all simulated profiles within the latitude grid of 70 and 90
569 degrees for each pole.

570 The observed abundance ratios demonstrate that in the south pole C_2H_2 , C_2H_6 , and C_3H_8 remain
571 approximately constant or slightly increase by factors < 2 within error bars over the period 2010-
572 2017, with the exception of the latest observation in 2014 that reveals an enhancement particularly
573 for C_2H_6 up to a factor of 3 relative to the 2010 abundance. For C_2H_4 , C_3H_4 , and C_4H_2 the increase of
574 their abundances towards 2014 is more pronounced starting from 2012 and reaching maximum values
575 of ~ 6 for C_2H_4 and C_3H_4 , while C_4H_2 increases by a factor of ~40 by 2014. Similarly, the 2017
576 observations reveal a clear decrease in the abundances of these species, with C_2H_4 reaching the 2010
577 abundance, while C_3H_4 and C_4H_2 dropping at about 2 times and 10 times the 2010 abundance. For
578 C_6H_6 , HCN and HC_3N the observations reveal the maximum effect of seasonal changes, with the
579 2014 ratios reaching values of ~100 for HCN and HC_3N , and ~2000 for benzene, while the rate of
580 increase is strongest for C_6H_6 and HC_3N , which by mid-2012 reveal enhancements factors of ~50-100
581 relative to the 2010 abundances. As with the other species, the abundance ratios drop in 2017, but
582 still remain higher by factors of ~8 (HCN), 20 (HC_3N), and 30 (C_6H_6) in August of 2017 relative to
583 2010. Over the north pole, observations between 2014 and 2017 reveal a consistent decrease in
584 abundances by factors ranging between 1 and 10, while as with the south pole HCN, HC_3N , and C_6H_6
585 demonstrate the strongest temporal variations.

586 When compared to the GCM results (Rannou et al., 2005), we find that the simulated circulation
587 provides a global picture that is consistent with the observations. The magnitude of temporal variation
588 observed for the various species is consistent with the anticipations based on the correlation with their
589 condensation level. Estimates for the altitudes where different species should condense in Titan's
590 atmosphere demonstrate that C_2H_2 , C_2H_4 , C_2H_6 , C_3H_4 , and C_3H_8 condense at similar altitudes below
591 60 km, HCN, HC_3N , and C_4H_2 near 75 km, while C_6H_6 near 85 km (see Fig. 1 in Lavvas et al., 2011).
592 Although these altitudes correspond to equatorial temperature conditions, the grouping of species will
593 remain similar at different temperatures, as their saturation vapor pressures dominantly control their
594 condensation levels. Thus, species within each of the above groups should demonstrate similar
595 magnitude temporal variations, as our observations reveal. However, there are subtle details not yet
596 captured by the models. Over the south pole and for most of the species, the temporal variation of the
597 mixing ratios is consistent with the observations, when these are of small (C_2H_2 , C_2H_4 , C_2H_6 , C_3H_8)
598 or moderate (C_3H_4 , C_4H_2) magnitude, but the model fails to capture the increase observed around
599 2014, as well as, the drop following it. The simulations provide a better description for the HCN
600 temporal variation capturing the increase in the abundance towards 2014 and the subsequent drop
601 with remarkable agreement in the magnitude, except at the peak value seen at the end of 2014 for
602 which the model is lower than the observation by a factor of ~10. For the other species demonstrating
603 a strong temporal variation (HC_3N , C_6H_6), the simulations do not capture the observed strong
604 enhancement or even the temporal variation. Over the north pole, the simulations capture the common
605 characteristic of abundance reduction (with the exception of C_2H_4), and provide results consistent
606 with the observations of C_2H_2 , C_2H_6 , C_3H_4 and C_3H_8 . However, for higher order hydrocarbons the
607 observed reduction in mixing ratios in 2016 and 2017 is higher than the GCM simulations.

608 We can further compare the temporal evolution of thermal structure from observations and
609 models (Fig. 8 upper panel). At the south pole the GCM suggests a continuous temperature increase
610 that reaches its maximum early in 2017 in the upper atmosphere, while the opposite behavior is
611 observed in the lower stratosphere. On the south pole, the upper stratosphere progressively cools
612 beyond 2013, reaching a quasi-isothermal profile above ~1 bar in August 2017, while at higher
613 pressures the opposite behavior of temperature rise is expected. Although these general characteristics
614 are consistent with the observations their magnitude is different. The upper stratosphere of the south
615 pole first passes through a temporal temperature decrease between June 2012 and at least September
616 2014, before increasing again towards the temperature maximum observed in 2017 (see Fig. 5a). This
617 different behavior relative to the models has also been seen in CIRS limb observations (Teanby et al.,
618 2017). At higher pressures, model and observations have a similar temporal discrepancy as at lower
619 pressures, but the general behavior of the simulations is more consistent with the observations.

620 These differences can be better demonstrated when comparing the temporal variations in the
621 average temperatures calculated over the full width at half maximum (FWHM) of the contribution
622 functions of the CH_4 Q, R and P branches (Fig. 8 lower panel). As shown in Fig. 4, each CH_4 branch
623 is sensitive to different parts of the atmosphere that varies with time. For the Q and P branches (the P

Supprimé: a

Supprimé: differences

Supprimé: with

Supprimé: b

628 branch not shown in Fig. 4 has a similar behavior to the Q branch), the contribution functions have
629 two broad peaks in the mid and lower stratosphere in 2010 and progressively shift towards a single
630 peak probing at 10 mbar by the end of 2014. However, the situation reflexes in 2017 with the Q and
631 P branches probing mainly the upper stratosphere near 0.05 mbar. Therefore, based on the observed
632 temperature profiles, the average temperature changes (relative to 2010) are negative until 2014 when
633 the temperature in the lower atmosphere drops in the south pole, and positive in 2017 as the
634 temperature in the upper stratosphere is higher relative to 2010. The corresponding GCM average
635 temperature differences do follow this behavior but with a different magnitude. The temperature drop
636 between 2010 and 2014 is smaller than the observed and reaches a maximum of ~ 10 K in mid 2012,
637 while the temperature rise in the upper atmosphere with a maximum in 2017 is ~ 50 K, i.e. more than
638 a factor of 2 larger than the observed. For the R branch the contribution function peaks near 0.5 mbar
639 in 2010 and progressively moves to lower pressures reaching to ~ 0.05 mbar in 2017. Thus,
640 observations demonstrate a negative temperature difference relative to the 2010 that decreases after
641 2014 but remains at negative values up to 2017. The corresponding average temperature changes for
642 the GCM are more symmetric and demonstrate a rapid increase in temperature after 2013 reaching to
643 $+35$ K by mid-2017.

644 At the north pole the contribution functions indicate a more stable with time variation. The Q
645 and P branches have a dominant contribution at 0.1 \sim mbar and a secondary near 5 mbar, while the R
646 branch has a single broad profile centered at ~ 0.2 mbar. As our retrieved north pole temperature
647 profiles are similar over the period under investigation the derived average temperatures are very
648 close thus resulting to small temperature differences. Although the simulations do demonstrate a
649 smaller temperature change in the north relative to the south pole, the simulated temperature decrease
650 is stronger than the observations for the Q and P branches, while for the R branch temperature rises
651 by about 30 K although the observations suggest temperature differences smaller than 5 K over the
652 observed period.

653 Along with the gases the circulation also enhances the haze abundance in the winter pole, which
654 has further implications for the thermal structure. Haze particles can locally cool the atmosphere, and
655 due to the lack of solar radiation this effect will be more important relative to lower latitudes where
656 heating by absorption of solar light balances the cooling. This mechanism could be relevant for the
657 stronger temperature gradient observed in the 2017 temperature retrievals if the haze accumulation is
658 higher at that time in the lower stratosphere.

659 In summary, our report here takes into account the whole pool of nadir high-resolution CIRS
660 polar spectra to the end of the mission in 2017 and aims to bring improved understanding of the
661 seasonal and temporal evolution of Titan's complex atmospheric system. We show strong variations
662 in the thermal and chemical structure of Titan near the south pole and significant ones near the
663 northern pole as they evolve seasonally, while the equatorial latitudes remain rather unaffected
664 throughout the Cassini mission. Using the very last data from Cassini, we set constraints on
665 photochemical and circulation models, which need to account for the asymmetry found in the poles'
666 behavior. A future space mission to Titan's complex system will have to complement the important
667 findings of the highly successful Cassini-Huygens mission and bring answers to the many new
668 questions it has raised, in particular concerning the organic chemistry and its evolution with time.

669 We have shown that the south pole of Titan is now losing its strong enhancement, while the
670 north pole also slowly continues its decrease in gaseous opacities and has not picked up again. It
671 would have been interesting to see when this might happen, but the Cassini mission ended in
672 September 2017. Perhaps future ground-based measurements can pursue this investigation and
673 monitor Titan's atmosphere to characterize the seasonal events.

674

675

676

677 **Acknowledgements**

678 The authors acknowledge support from NASA's Cassini mission and Cassini data Analysis
679 program, as well as from the French Centre National d'Etudes Spatiales.

680

681

682

683 **References**

684

685 [Achterberg, R.K., Conrath, B.J., Gierasch, P.J., Flasar, F.M., Nixon, C.A., 2008. Titan's middle-
686 atmospheric temperatures and dynamics observed by the Cassini Composite Infrared
687 Spectrometer. *Icarus* 194, 263-277.](#)

688 Achterberg, R.K., Gierasch, P.J., Conrath, B.J., Flasar, F.M., Nixon, C.A., 2011. Temporal variations
689 of Titan's middle-atmospheric temperatures from 2004 to 2009 observed by Cassini/CIRS.
690 Icarus 211, 686-698.

691 Bampasidis, G., et al., 2012. Thermal and chemical structure variations in Titan's stratosphere during
692 the Cassini mission. *Astroph. J.*, 760 (2), 8 pp 144.

693 Conrath, B.J., Gierasch, P.J., Ustinov, E.A., 1998. Thermal structure and para hydrogen fraction on
694 the outer planets from Voyager IRIS measurements. *Icarus* 135, 501–517.

695 Coustenis, A., et al., 2007. The composition of Titan's stratosphere from Cassini/CIRS mid-infrared
696 spectra. *Icarus* 189, 35-62.

697 Coustenis, A., et al., 2010. Titan trace gaseous composition from CIRS at the end of the Cassini–
698 Huygens prime mission. *Icarus* 207, 461–476.

699 Coustenis, A., et al., 2013. Evolution of the stratospheric temperature and chemical composition over
700 one Titanian year. *Astrophys. J.* 779, 177, 9 pp.

701 Coustenis, A., et al., 2016. Titan's temporal evolution in stratospheric trace gases near the poles.
702 *Icarus* 270, 409–420.

703 Coustenis, A., et al., 2018. Seasonal Evolution of Titan's Stratosphere Near the Poles. *Astrophys. J.*
704 *Lett.* 854, L30, 7 pp.

705 Flasar, F.M., et al., 2004. Exploring the Saturn system in the thermal infrared: The Composite Infrared
706 Spectrometer. *Space Sci. Rev.* 115, 169-297.

707 Flasar, F.M., et al., 2005. Titan's atmospheric temperatures, winds, and composition. *Science* 308,
708 975-978.

709 Hourdin, F., Lebonnois, S., Luz, D., Rannou, P., 2004. Titan's stratospheric composition driven by
710 condensation and dynamics. *J. Geophys. Res.* 109 (E), E12005, 15 pp.

711 Jennings, D.E. et al., 2012a. Seasonal disappearance of far-infrared haze in Titan's stratosphere.
712 *Astrophys. J.* 754, L3, 4 pp.

713 Jennings, D.E. et al., 2012b. First observation in the south of Titan's far-infrared 220 cm⁻¹ cloud.
714 *Astrophys. J.* 761, L15, 4 pp.

715 Jennings, D. et al., 2015. Evolution of the far-infrared ice cloud at Titan's south pole. *Astrophys. J.*
716 804, L34, 5 pp.

717 Jennings, D.E., et al., 2017. Composite infrared spectrometer (CIRS) on Cassini. *Apl. Opt* 56, 5274-
718 5294.

719 Lacis, A.A., Oinas, V., 1991. A description of the correlated k distribution method for modeling
720 nongray gaseous absorption, thermal emission, and multiple scattering in vertically
721 inhomogeneous atmospheres. *J. Geophys. Res.* 96 (D5), 9027–9063.

722 Lavvas, P. P., Coustenis, A. & Vardavas, I. M., 2007. Coupling photochemistry with haze formation
723 in Titan's atmosphere, Part I: Model description. *Plan. Space Sci.* 56, 27-66.

724 Lavvas, P. P., Coustenis, A. & Vardavas, I. M., 2008. Coupling photochemistry with haze formation
725 in Titan's atmosphere, Part II: results and validation with Cassini/Huygens data. *Plan. Space*
726 *Sci.* 56, 67–99.

727 Lavvas, P., Griffith, C.A., Yelle, R.V., 2011. Condensation in Titan's atmosphere at the Huygens
728 landing site. *Icarus* 215, 732-750.

729 Lebonnois, S., Rannou, P., Hourdin, F., 2009. The coupling of winds, aerosols and chemistry in
730 Titan's atmosphere. *Philosoph. Trans. Royal Soc. A* 367, 665-682.

731 Lebonnois, S., Burgalat, J., Rannou, P., Charnay, B., 2012. Titan global climate model: A new 3-
732 dimensional version of the IPSL Titan GCM. *Icarus*, 218, 707-722.

733 Lora, J.M., Lunine, J.I., Russell, J.L., 2015. GCM simulations of Titan's middle and lower atmosphere
734 and comparison to observations. *Icarus* 250, 516-528.

735 Niemann, H.B., et al., 2010. Composition of Titan's lower atmosphere and simple surface volatiles
736 as measured by the Cassini-Huygens probe gas chromatograph mass spectrometer
737 experiment. *J. Geophys. Res.* 115, E12006, 22 pp.

738 Nixon, C.A., Ansty, T. M., Lombardo, N. A., et al, 2019, *Astroph. J. Supp. Series*, in press.

739 Rannou, P., Lebonnois, S., Hourdin, F., Luz, D., 2005. Titan atmosphere database. *Adv. Space Res.*
740 36, 2194–2198.

741 Sylvestre, M., Teanby, N.A., Vinatier, S., Lebonnois, S., Irwin, P.G.J., 2018. Seasonal evolution of
742 C₂N₂, C₃H₄, and C₄H₂ abundances in Titan's lower stratosphere. *Astron. Astrophys.* 609, A64
743 13 pp.

744 Sylvestre, M., Teanby, N.A., Vatan d'Ollone, J., Vinatier, S., Bezard, B., Lebonnois, S., Irwin,
745 P.G.J., 2019. Seasonal evolution of temperatures in Titan's lower stratosphere, submitted.

746 Teanby, N.A., et al., 2012. Active upper-atmosphere chemistry and dynamics from polar circulation
747 reversal on Titan. *Nature* 491, 732-735.

748 Teanby, N. A., Bézard, B., Vinatier, S., et al., 2017. The formation and evolution of Titan's winter
749 polar vortex. *Nature Comm.* 8, 1586, 13 pp.

750 Teanby, N.A., et al., 2018. The origin of Titan's external oxygen: further constraints from ALMA
751 upper limits on CS and CH₂NH. *Astron. J.* 155, 251, 8 pp.
752 Vinatier, S., et al., 2015. Seasonal variations in Titan's middle atmosphere during the northern spring
753 derived from Cassini/CIRS observations, *Icarus* 250, 95-115.
754 Vinatier, S., Schmitt, B., Bézard, B., Rannou, P., Dauphin, C., de Kok, R., Jennings, D. E., Flasar, F.
755 M., 2018. Study of Titan's fall southern stratospheric polar cloud composition with
756 Cassini/CIRS: Detection of benzene ice. *Icarus* 310, 89-104.
757 Vuitton, V., Yelle, R. V., Klippenstein, S. J., Hörst, S. M., Lavvas, P., 2019. Simulating the density
758 of organic species in the atmosphere of Titan with a coupled ion-neutral photochemical model.
759 *Icarus* 324, 120-197.
760 West, R.A., et al., 2011. The evolution of Titan's detached haze layer near equinox in 2009. *Geophys.*
761 *Res. L.* 38, L06204, 4 pp.
762 West, R.A., et al., 2016. Cassini Imaging Science Subsystem observations of Titan's south polar
763 cloud, *Icarus* 270, 399-408.
764
765

Table 1
FP3 SPECTRAL SELECTIONS

<i>south pole</i>						
Year	Month	Latitudinal bin	Number of spectra	Airmass	COMPMAP	Ls (°)
2017	February	70°S to 90°S	1505	1.423	CIRS_259TI_COMPMAP001_PIE CIRS_259TI_COMPMAP002_PRIME	87
2017	February	68°S to 70°S	151	1.231	CIRS_259TI_COMPMAP001_PIE CIRS_259TI_COMPMAP002_PRIME	87
2017	June	65°S to 90°S	228	1.798	CIRS_280TI_COMPMAP001_PIE	91

<i>north pole</i>						
Year	Month	Latitudinal bin	Number of spectra	Airmass	COMPMAP	Ls (°)
2017	February	65°N to 90°N	868	1.094	CIRS_261TI_MIDIRTMAP001_PRIME	87
2017	July	65°N to 90°N	2694	1.244	CIRS_283TI_COMPMAP001_PRIME CIRS_283TI_COMPMAP002_PRIME CIRS_283TI_COMPMAP003_PRIME	91
2017	August	65°N to 90°N	6667	1.249	CIRS_288TI_COMPMAP002_PIE CIRS_288TI_COMPMAP003_PIE	92
2017	September	65°N to 90°N	1920	1.222	CIRS_292TI_COMPMAP001_PRIME CIRS_293TI_COMPMAP002_PRIME	93

<i>equator</i>						
Year	Month	Latitudinal bin	Number of spectra	Airmass	COMPMAP	Ls (°)
2017	Feb-Sept	10°S to 10°N	902	1.218	*	87-93

FP4 SPECTRAL AVERAGES

<i>south pole</i>						
Year	Month	Latitudinal bin	Number of spectra	Airmass	COMPMAP	Ls (°)
2017	February	70°S to 90°S	1505	1.423	CIRS_259TI_COMPMAP001_PIE CIRS_259TI_COMPMAP002_PRIME	87
2017	February	68°S to 70°S	151	1.231	CIRS_259TI_COMPMAP001_PIE CIRS_259TI_COMPMAP002_PRIME	87
2017	June	65°S to 90°S	231	1.793	CIRS_280TI_COMPMAP001_PIE	91

<i>north pole</i>						
Year	Month	Latitudinal bin	Number of spectra	Airmass	COMPMAP	Ls (°)
2017	February	65°N to 90°N	825	1.102	CIRS_261TI_MIDIRTMAP001_PRIME	87
2017	July	65°N to 90°N	2707	1.247	CIRS_283TI_COMPMAP001_PRIME CIRS_283TI_COMPMAP002_PRIME CIRS_283TI_COMPMAP003_PRIME	91
2017	August	65°N to 90°N	7089	1.222	CIRS_288TI_COMPMAP002_PIE CIRS_288TI_COMPMAP003_PIE	92
2017	September	65°N to 90°N	1935	1.190	CIRS_292TI_COMPMAP001_PRIME CIRS_293TI_COMPMAP002_PRIME	93

<i>equator</i>						
Year	Month	Latitudinal bin	Number of spectra	Airmass	COMPMAP	Ls(°)
2017	Feb-Sept	10°S to 10°N	975	1.168	*	87-93

*Our equatorial selections are spectral averages from all the datasets mentioned here in polar latitudes.

Table 1. This table shows the high resolution data taken in nadir mode near the south and north poles of Titan in focal planes 3 and 4 of the CIRS instrument. Ls is the solar longitude at the time of the observation. The distance to the satellite from the spacecraft is up to 400,000 km. In our previous papers, we refer to specific Titan close flybys in our selection tables. In this paper, we model CIRS spectra acquired from distant Titan flybys during Cassini Grand Finale mission and we use the COMPMAP parameter to identify them.

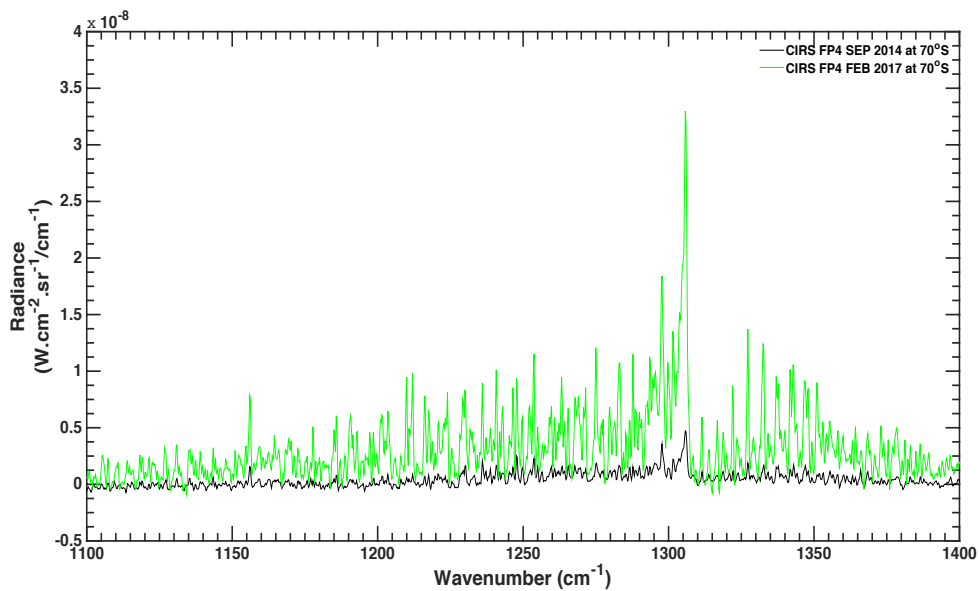


Figure 1: comparison between September 2014 (black lines) and February 2017 (green lines) CIRS nadir spectra in the FP4 at high southern latitudes. The strong emission at 1304 cm^{-1} is due to the Q-branch of methane, and the peak at 1161 cm^{-1} is due to CH_3D . The September 2014 70°S data contain an average of 1187 spectra with an airmass of 1.2, the Feb 2017 70°S average has 151 spectra summed up for an airmass of 1.23, so the two datasets are at similar geometry conditions and can be compared. The differences indicate at a glance considerably stronger emission in the center and the wings of the CH_4 band in 2017 which is indicative of much higher temperatures in the south with respect to 2014. The purpose of the present work is to quantify such seasonal changes in temperature and composition. In this Figure and the following ones of this type, we restrain the longer wavenumber range to 1400 cm^{-1} for clarity purposes and because no exploitable information was retrieved here from the emission beyond that.

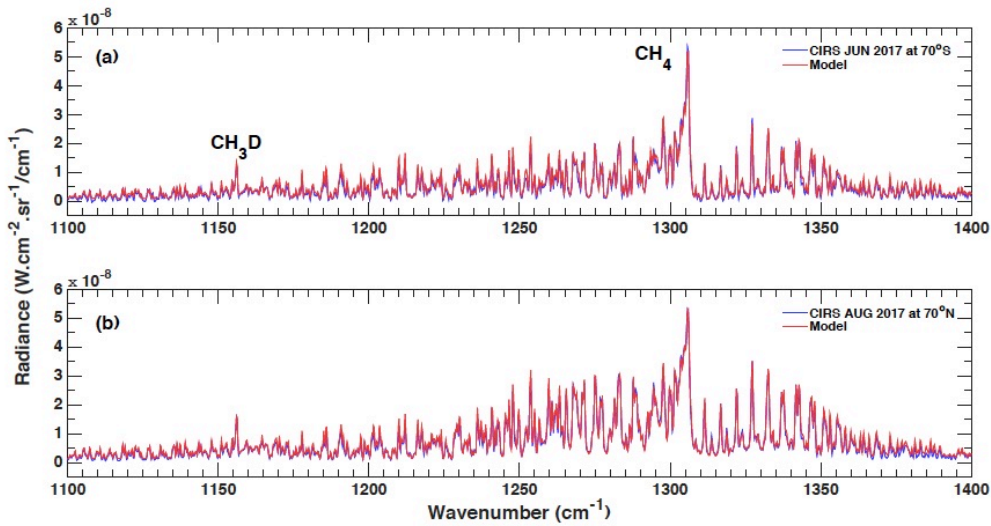


Figure 2: Sample of fits in the 1200-1400 cm^{-1} part (FP4) of the Titan spectrum containing the CH_4 emission band at $7.7 \mu\text{m}$ which gives access to the temperature profile in the stratosphere. The blue curves are the CIRS observations in August 2017 at 75°N (top) and June 2017 at 70°S (bottom) and the red curves are the model simulations that best fit the data.

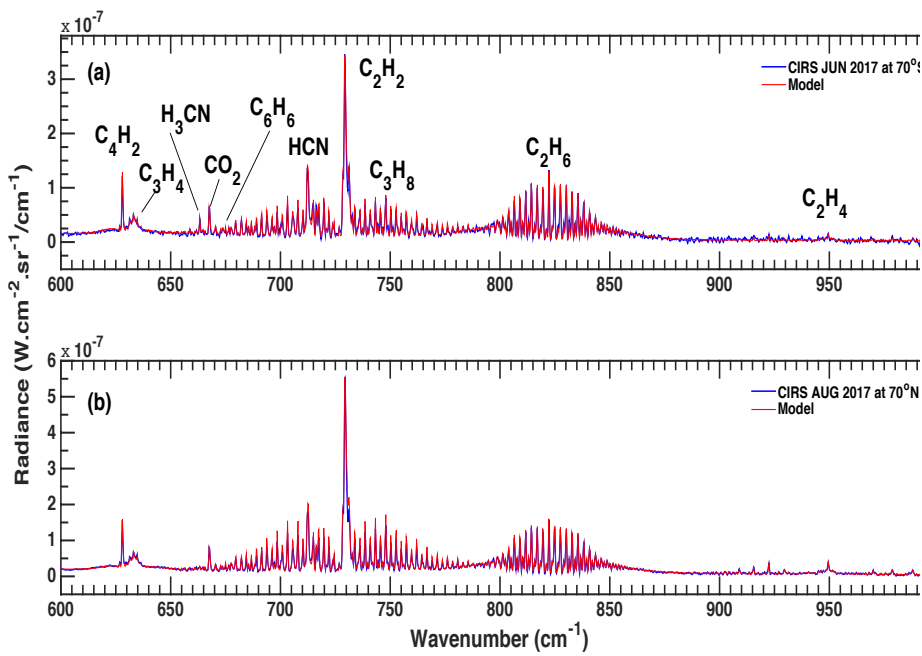


Figure 3: Same as Figure 2, but for a sample of fits in the 600-1000 cm^{-1} , part of the FP3 Titan spectrum, where the spectral signatures of several of hydrocarbons and an oxygen compound exist as indicated.

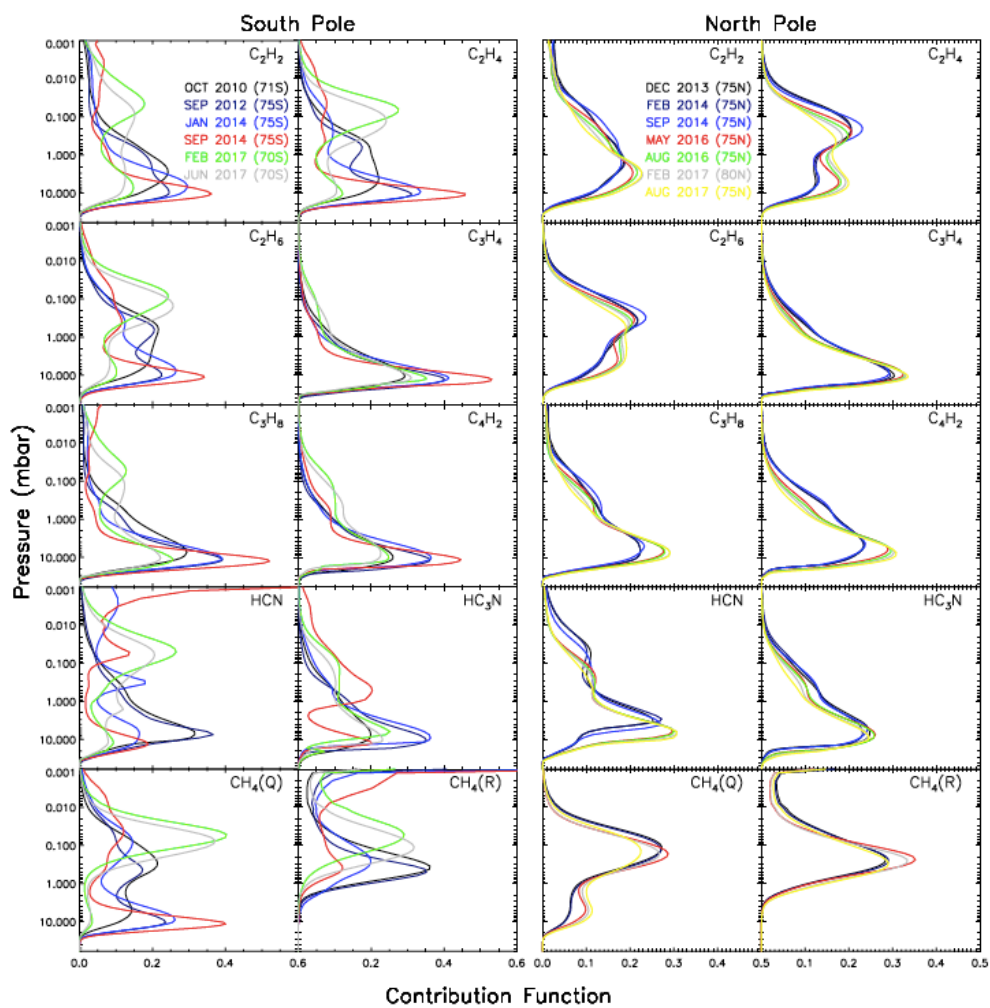


Figure 4: Contribution functions for the species observed in Titan's stratosphere near the South Pole (left two columns) and the North Pole (right two columns). Lower four cells : contribution functions for the emission observed in the methane band in FP4 centered at 1305 cm^{-1} (Q-branch) and in the R branch (1250 cm^{-1}). The dates are given in the upper panels. For the corresponding altitude levels see Fig. 5.

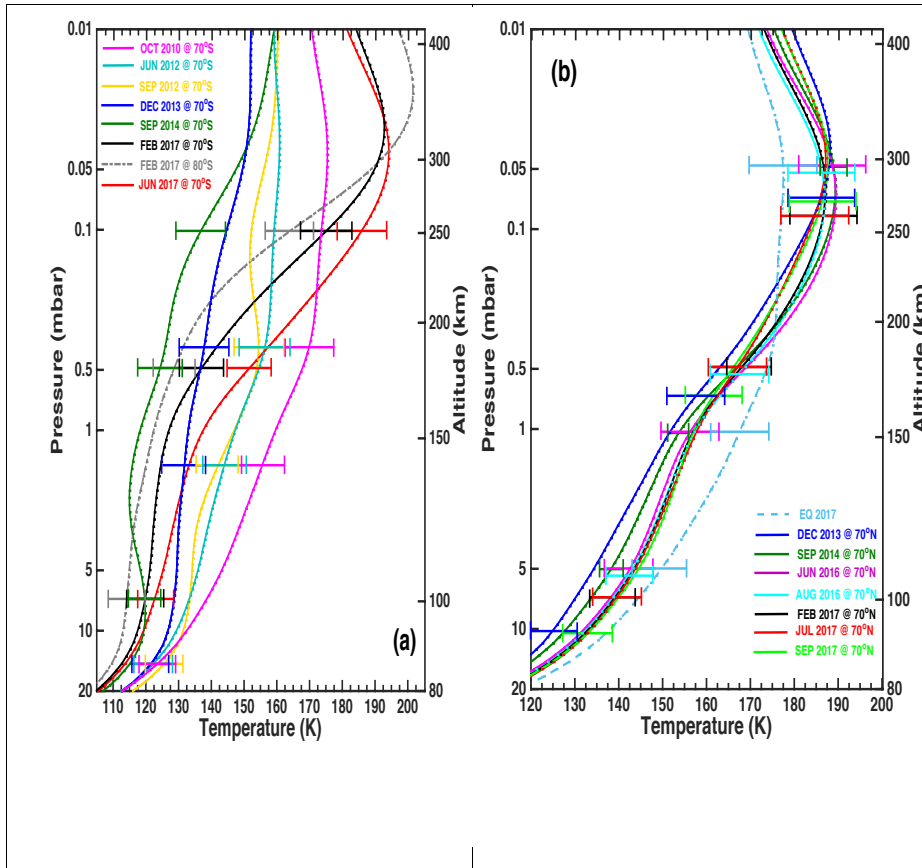


Figure 5: Temperature evolution in Titan's stratosphere : a) near the south pole from 2010 to 2017; b): from end of 2013 to 2017 near the north pole. The different dates are indicated in different colors. The averaged equatorial thermal profile for 2017 is also plotted in dotted lines in (b). 3- σ uncertainties on the temperatures are shown with the horizontal bars at different pressure levels for clarity.

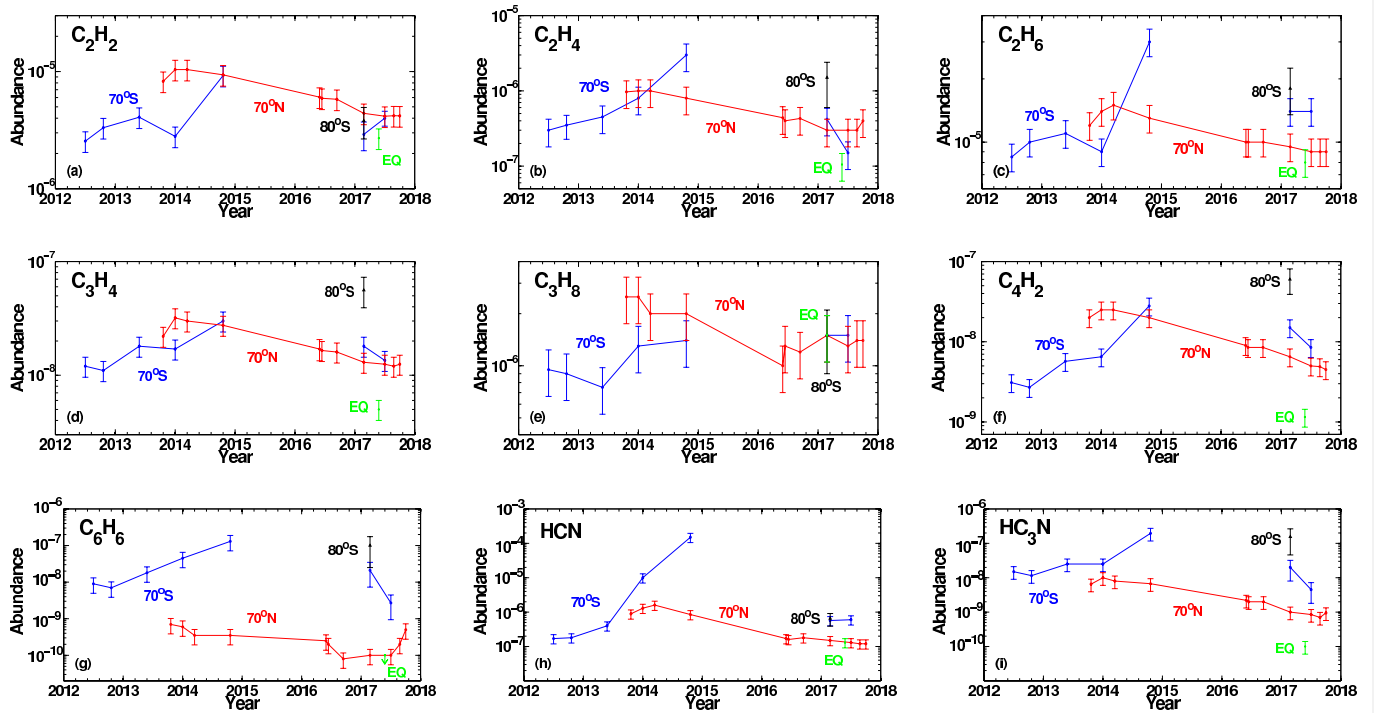


Figure 6 : Abundances of trace hydrocarbon and nitrile gases in the stratosphere of Titan from 2012 to 2017 for the south polar region near 70°S (blue lines) and some exceptional data taken near 80°S in February 2017 (black points), for the north polar region (red lines-near 70°N) and an equatorial average in 2017 from -10° to +10° as green points. Note that we have no FP3 nadir data between 2014 and 2017 for the south polar region and that therefore the connecting blue lines are not interpolated (see table for detailed description of selections). 3-sigma error bars are indicated.

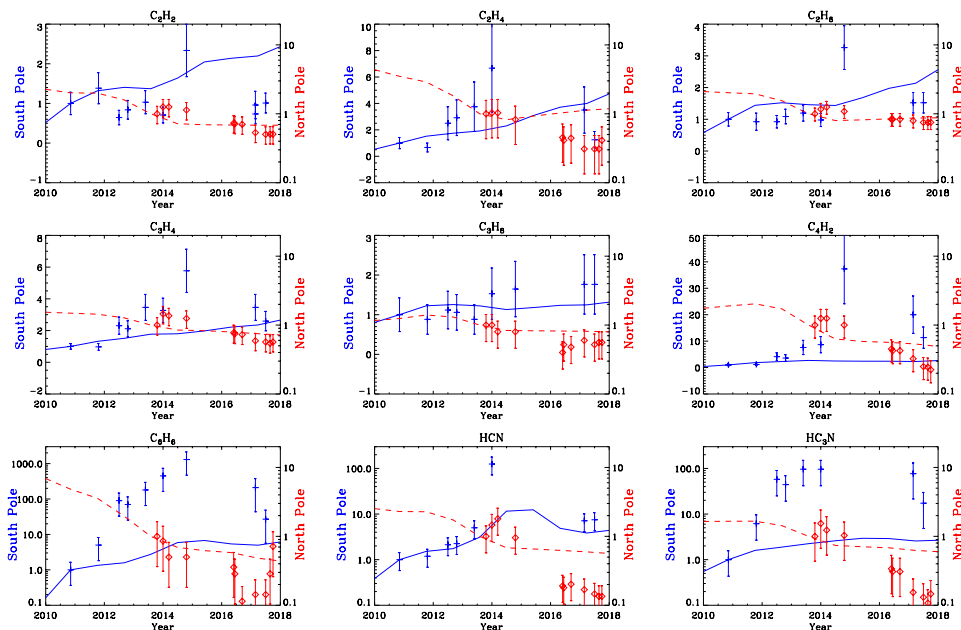


Figure 7 : Seasonal evolution of the mixing ratios over the polar regions normalized to the 2010 and 2013 observations for the South (in blue) and North (in red) pole, respectively. Symbols with error bars present the CIRS observations and lines the GCM simulations (database by Rannou et al., 2005). The scale on the left is the ratio of mixing ratios $x(t)/x(2010)$ for the south pole (blue curves/points) and the scale on the right the corresponding ratio $x(t)/x(2013)$ for the north pole (red).

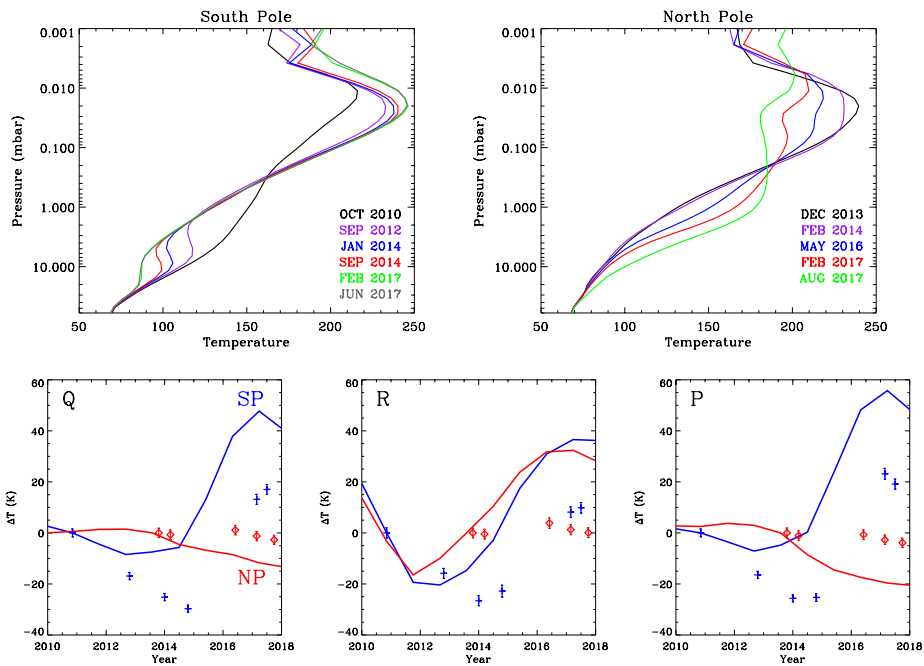


Figure 8: (upper panel): temporal evolution of the thermal structure as found by GCM models; (lower panel): comparison between the CIRS observations acquired at the dates shown in the upper panel and the temporal differences in the average temperatures calculated with the contribution functions of the methane band Q, R and P branches.

Supprimé: Comparison of the

Supprimé: as seen in the CIRS observations and

Supprimé: of